An improved derivation of the top-of-atmosphere albedo from POLDER/ADEOS-2: 2. Broadband albedo

Jean-Claude Buriez, Frédéric Parol, Z. Poussi, Michel Viollier

An improved derivation of the top-of-atmosphere albedo from POLDER/ADEOS-2: 2. Broadband albedo

Jean-Claude Buriez,[1] Frédéric Parol,[1] Zegbeu Poussi,[2] and Michel Viollier[3]

Received 15 November 2006; revised 28 March 2007; accepted 5 July 2007; published 10 October 2007.

[1] The narrowband albedos derived from Polarization and Directionality of Earth Reflectances (POLDER) measurements have been described in a companion paper (Buriez et al., 2005). Here, they are used to estimate the broadband shortwave albedo. Except for the gaseous absorption, the albedos at 443 and 670 nm are considered as representative of the UV-visible range, and the albedo at 865 nm is considered as representative of the near infrared. The gaseous absorption is estimated from TOMS data and from the POLDER 910- to 865-nm reflectance ratio. In a previous approach, the respective weights of the three narrowband albedos were based on radiative transfer simulations. Now, we take advantage of spatiotemporal coincidences between the second Advanced Earth Observing Satellite (ADEOS-2) and Terra to adjust these weights from the comparison between POLDER narrowband and CERES broadband reflectances. With no adjustment, the POLDER albedos are underestimated by 2% (in relative value) whereas the associated reflectances are underestimated by 4%. With an adjustment to the CERES reflectances, the POLDER shortwave albedos are overestimated by 2%. With or without adjustment the RMS difference between the POLDER and the CERES 1°-regional instantaneous shortwave albedos is 6%; this is quite satisfactory since it is comparable to the CERES SW albedo consistency between nadir and oblique viewing zenith angles. When considering only homogeneous areas, the agreement between POLDER and CERES estimates was rather less good in the previous approach; it is now more than twice better. The difference between POLDER and CERES shortwave albedo estimates appears, for a large part, due to our plane-parallel assumption that is crucial for the heterogeneous liquid water clouds. It results in a bias in monthly mean shortwave flux around 2 W m^{-2} that is found to present only small variations in latitude.

Citation: Buriez, J.-C., F. Parol, Z. Poussi, and M. Viollier (2007), An improved derivation of the top-of-atmosphere albedo from POLDER/ADEOS-2: 2. Broadband albedo, *J. Geophys. Res.*, *112*, D19201, doi:10.1029/2006JD008257.

1. Introduction

[2] Polarization and Directionality of the Earth's Reflectances (POLDER) [*Deschamps et al.*, 1994] has demonstrated new methods of remote sensing in different fields: ocean color, land surface, cloud and aerosol properties. It can also contribute to the determination of the Earth Radiation Budget (ERB) by improving the estimate of the reflected shortwave (SW) radiation. Thanks to its multi-angle observations, POLDER obtains direct information on the anisotropy of the reflected radiation field. However, because of the lack of a broadband solar channel, POLDER is not an ERB-dedicated instrument such as the Scanner for Radiation Budget (ScaRaB) [*Kandel et al.*, 1998] and the Clouds and the Earth's Radiant Energy System (CERES) [*Wielicki et al.*, 1996].

[3] Narrowband albedos at top of the atmosphere (TOA) can be derived from POLDER measurements at 443, 670, and 865 nm, as reported in the first part of this series [*Buriez et al.*, 2005] (hereinafter referred to as Part 1). They can be used to estimate the broadband SW albedo. However, the calibration and/or the validation of these SW albedo values need a comparison with broadband ERB measurements.

[4] Before the launch of the first Advanced Earth Observing Satellite (ADEOS-1) in 1996, a comparison between POLDER and ScaRaB was scheduled. Unfortunately, during the period ADEOS-1 POLDER was working (November 1996 to June 1997), there was neither ScaRaB nor any ERB scanner in flight. Nevertheless, solar reflected fluxes were computed for the eight months of ADEOS-1 POLDER [*Viollier et al.*, 2002]. Results were very encouraging since the mean SW reflected fluxes were found to be in good agreement (within 3–7%) with climatological

[1] Laboratoire d'Optique Atmosphérique, UMR CNRS 8518, Université des Sciences et Technologies de Lille, Villeneuve d'Ascq, France.
[2] Centre de Gestion et de Traitement des Données, Interactions Clouds Aerosols Radiations Etc., Université des Sciences et Technologies de Lille, Villeneuve d'Ascq, France.
[3] Laboratoire de Météorologie Dynamique, CNRS, Ecole Polytechnique, Palaiseau, France.

0148-0227/07/2006JD008257

values, despite the lack of "calibration" of the POLDER SW flux estimates.

[5] Since then, a second POLDER instrument, identical to the first one, was functioning nominally aboard ADEOS-2 from April 2003 to October 2003. During this period, CERES instruments were orbiting aboard the Earth Observing System (EOS) spacecrafts Terra and Aqua. As Terra and ADEOS-2 are polar orbiting platforms with the same descending local crossing time, there are good opportunities for the comparison between ADEOS-2 POLDER and Terra CERES observations.

[6] CERES and POLDER data used in this study are presented in section 2. The method of narrowband-to-broadband conversion developed for POLDER is described in section 3. Regression coefficients are determined as explained in section 4. It results in POLDER SW reflectance and albedo estimates that are compared to CERES data in sections 5 and 6. Conclusions are drawn in section 7.

2. CERES and POLDER Data

[7] The POLDER instrument was functioning nominally aboard ADEOS-2 only from April 2003 to October 2003. During this period, two CERES instruments, Flight Models 1 (FM-1) and 2 (FM-2), were operational aboard the Terra spacecraft, launched in December 1999. The altitude of ADEOS-2 and Terra is about 800 km and 700 km, respectively. Both satellites are in a descending Sun-synchronous orbit with an equator crossing time of 1030 local time. It results in quasi-coincidences between ADEOS-2 and Terra orbits about once every 3 days. In the following, only quasi-simultaneous data are retained: measurements must to be acquired within 10 min of each other.

[8] POLDER is a camera composed of a wide field-of-view lens, a rotating wheel carrying spectral filters and polarizers, and a coupled device detector (CDD) array of 242 $\times$ 274 detectors that induces a spatial resolution of 6.2 km. As the satellite moves over a region, up to 14 successive measurements are acquired in eight narrow spectral bands located between 443 and 910 nm. Unlike many spaceborne radiometers, the POLDER instrument has no internal calibration source. However, in-flight calibration is ensured by many calibration methods using well-characterized targets [*Hagolle et al.*, 1999]. The absolute accuracy of the ADEOS-2 POLDER reflectances is estimated to be about 2% for all the spectral bands, except for the 443 nm band for which there is still unexplained discrepancies between different calibration methods (http://smsc.cnes.fr/POLDER/A_calibration.htm). Here we make use of data issued from the POLDER "ERB, water vapor and clouds" level 2 processing line (see Part 1). These data consist in particular of narrowband reflectances and albedos at 443 nm, 670 nm and 865 nm over a regular geographical grid of 18.5 $\times$ 18.5 km^2 corresponding to level 2 pixels (composed of 3 $\times$ 3 level 1 pixels and denoted as "superpixels" in Part 1). The derivation of narrowband albedos from POLDER reflectances is based on plane-parallel radiative transfer modeling. For oceanic areas, the sea surface reflectance is calculated by using the *Cox and Munk* [1956] model. For continental areas, the surface reflectance is issued from 10-day synthesis of POLDER data [*Hautecoeur and Leroy*, 1998]. Aerosol properties are derived from the Aerosol Robotic Network (AERONET) observations [*Dubovik et al.*, 2002]. Clouds are assumed to be composed of liquid water droplets or inhomogeneous hexagonal ice crystals [*C.-Labonnote et al.*, 2001], depending on the cloud thermodynamic phase derived from POLDER polarization measurements [*Goloub et al.*, 2000]. Practically, look-up tables of reflectances and albedos are used for the reflectance-to-albedo conversion that is widely described in Part 1. Note that as the POLDER instrument observes a given scene under several viewing directions, different "directional" albedo values can be retrieved. These values are finally averaged using angle-weighted functions, which are based on the statistical analysis of a large set of ADEOS-1 POLDER data. The nondirectional albedo values are found to be statistically a few better than the directional values (see Part 1).

[9] CERES instruments measure filtered radiances in three wavelength ranges between 0.2 μm and 5 μm, between 0.2 μm and 100 μm, and between 8 μm and 12 μm. These filtered radiances are converted into unfiltered radiances, including the SW radiance with a relative error generally below 1% [*Loeb et al.*, 2001]. The shortwave reflectance R_{sw} can be directly deduced from

$$R_{sw} = \pi L_{sw}/\mu_s E_o(d) \quad (1)$$

where μ_s is the cosine of solar zenith angle and $E_o(d)$ is the solar irradiance outside the atmosphere corrected for the Earth-Sun distance for the day d of the year, with an annual mean value of 1365 W m^{-2}.

[10] CERES scanners present the ability to operate in different scan modes. Here we make use of data from the FM-1 instrument, which was operating in a standard cross-track mode during the relevant period. Data are issued from the CERES Terra Edition2B-Rev1 Single Scanner Footprint TOA/Surface Fluxes and Clouds (SSF) product [*Geier et al.*, 2003]. This product combines CERES measurements with scene information from Moderate Resolution Imaging Spectroradiometer (MODIS) [*Salomonson et al.*, 1989; *Barnes et al.*, 1998], which is also on Terra. This scene information is used when measured radiances are converted into TOA radiative fluxes by means of empirical angular distribution models (ADMs) [*Loeb et al.*, 2005]. These radiative fluxes and other parameters are given at the CERES footprint resolution that is approximately 20 km (equivalent diameter) at nadir. The shortwave albedo A_{sw} is related to the SW flux F_{sw} by

$$A_{sw} = F_{sw}/\mu_s E_o(d). \quad (2)$$

Note that the comparison between CERES and POLDER albedos is relatively easy as the footprint geolocation is defined using a surface reference level for both CERES and POLDER products. The CERES fluxes are calculated at this reference level and then adjusted to the 20-km reference level in order to take into account the horizontal transmission of solar radiation through the atmosphere. Such an adjustment is not needed for POLDER as the albedo derivation described in Part 1 is based on the plane-parallel model that assumes no horizontal transmission (see *Loeb et al.* [2002] for further details).

[11] CERES and POLDER level 2 products correspond to comparable spatial resolution of about 20 km, but not strictly identical footprints. In order to reduce the influence of these spatial differences, CERES and POLDER reflectances and albedos are averaged into equal-area cells whose size at the equator is 1° in latitude and longitude. At least 80% of a cell area must be covered by both POLDER and CERES footprints. Snow covered and iced areas are excluded because the POLDER narrowband albedos are not derived over such surfaces.

[12] For reflectance comparisons, supplementary constraints are needed. CERES and POLDER observations must correspond to quasi-identical viewing geometry. To do that, we select the cases where the angle between the CERES and the POLDER viewing direction is weaker than 5°. Moreover, as the reflectance can vary very rapidly with viewing angle within the region of solar specular reflection, measurements that could be affected by sunglint are excluded. Practically, as the sunglint criterion is not exactly the same in the CERES and the POLDER algorithm, areas are excluded if one or the other data is labeled as "sunglint."

[13] For the narrowband to broadband regressions presented in the following, we have used the coincident data from CERES and POLDER for April, July and October 2003. There are 94,871 cells of 1° that fulfill the above-mentioned time and space criteria (time lag <10 min; angle between viewing directions <5°; no snow; no sunglint). These data that are well distributed over the three months correspond to 61,431 cells over oceans and 33,440 cells over continents.

3. Principle of the Narrow-to-Broadband Conversion

[14] Generally, the narrowband-to-broadband (NB-BB) conversion is applied to reflectances by using coincident measurements from a narrowband radiometer and an ERB scanner; then, the broadband reflectances are converted into broadband albedos and fluxes by means of ADMs [*Minnis and Harrison*, 1984; *Vesperini and Fouquart*, 1994; *Hucek and Jacobowitz*, 1995; *Minnis et al.*, 1995; *Duvel et al.*, 2000; *Viollier et al.*, 2004; *Loeb et al.*, 2006]. In other cases, the narrowband reflectances are first converted into albedos; then, the narrowband albedos are converted into broadband albedos by using regression coefficients derived from a set of narrowband and broadband albedos estimated from simultaneous data [*Trishchenko and Li*, 1998; *Li and Trishchenko*, 1999]. In the present work, the NB-BB conversion is also applied to albedos but by using a NB-BB regression derived from narrowband and broadband reflectances (not albedos). Indeed, while the SW radiance values derived from CERES instruments are very accurate (within 1% according to *Loeb et al.* [2001] and *Wielicki et al.* [2002]), the CERES instantaneous SW flux estimates suffer from errors in scene identification and angular distribution models, even if important progress has been made recently [*Loeb et al.*, 2005, 2007]. Our aim is to derive the regression coefficients from CERES and POLDER reflectance measurements and to make use of these coefficients to estimate the SW albedos from POLDER data. By doing so, the POLDER SW albedo estimates are independent from CERES except for calibration.

[15] As our NB-BB regression has to be transferred from reflectances to albedos, it must be physically comprehensible and robust. The bases of this NB-BB conversion applied to POLDER data have been very shortly described by *Buriez et al.* [1997] and are detailed in the following.

3.1. Shortwave Reflectances

[16] A given scene is observed nearly simultaneously from POLDER under up to 14 different viewing directions. Let us consider a viewing geometry represented by (μ_s, μ_v, φ), where μ_s and μ_v are the cosine of the solar and viewing zenith angles and φ the relative azimuth angle. Three POLDER spectral channels dedicated to aerosol, cloud and ERB studies are weakly affected by gaseous absorption. They are centered at 443, 670, and 865 nm, respectively. Let be $R_{443}(\mu_s, \mu_v, \varphi)$, $R_{670}(\mu_s, \mu_v, \varphi)$ and $R_{865}(\mu_s, \mu_v, \varphi)$ the corresponding TOA reflectances corrected for gaseous absorption as in the work by *Buriez et al.* [1997]. Except for the gaseous absorption, these reflectances are assumed to be representative of the entire shortwave range, the two first for the UV-visible part and the last one for the near-infrared part. In order to take into account the gaseous absorption that is chiefly due to ozone in the UV-visible and to water vapor in the near infrared, the SW reflectance is written as

$$R_{sw}(\mu_s, \mu_v, \varphi) = [C_1 R_{443}(\mu_s, \mu_v, \varphi) + C_2 R_{670}(\mu_s, \mu_v, \varphi)] \cdot T_{vis}(mU_{03}) + c_3 R_{865}(\mu_s, \mu_v, \varphi) T_{nir} \quad (3)$$

where C_1, C_2, and c_3 are constants. The function T_{vis} (T_{nir}) represents the ozone (water vapor) transmission weighted by the solar incident irradiance in the interval 0.2–0.7 μm (0.7–5 μm).

[17] The function T_{vis} is based on ozone transmission simulations [*Anderson et al.*, 1990] and is well approximated (within 0.01%) by means of Padé approximants [*Baker*, 1965]. It depends on the product mU_{03} where m is the air mass factor ($m = 1/\mu_s + 1/\mu_v$) and U_{03} the vertical column of ozone derived from the Total Ozone Mapping Spectrometer (TOMS) observations made aboard ADEOS-2. The major uncertainty related to the use of T_{vis} certainly comes from the fact that the spectral ozone transmission should be weighted not only by the spectral solar flux but also by the spectral scene reflectivity. Typically, it results in an uncertainty around 1%.

[18] The function T_{nir} that represents the broadband water vapor transmission is related to the water vapor transmission observed in the 910 nm region. Practically, T_{nir} is assumed to be a linear function of the ratio ρ_{H2O} between the 910 and 865 nm measured (uncorrected) reflectances,

$$T_{nir} = A + B\rho_{H2O}(\mu_s, \mu_v, \varphi) \quad (4)$$

where A and B are constants. Such a linear relation can be considered as very approximate. However, in the following, the use of several more complex functions was found to give no significant improvement from simulations as well as from comparisons between CERES and POLDER observations. Equation (4) can be physically interpreted in the following way: the whole near infrared transmission is a

combination of spectral intervals that are either practically not affected by the water vapor absorption (with a contribution A), either moderately affected and well represented by ρ_{H2O} (with a contribution B), or so strongly affected that the transmission is practically zero (with a contribution $1-A-B$).

[19] Finally, the broadband TOA reflectance can be related to the POLDER narrowband reflectances by using a multilinear regression method,

$$R_{sw}(\mu_s,\mu_v,\varphi) = [C_1\,R_{443}(\mu_s,\mu_v,\varphi) + C_2\,R_{670}(\mu_s,\mu_v,\varphi)] \cdot T_{vis}(mU_{03}) + C_3\,R_{865}(\mu_s,\mu_v,\varphi) + C_4\,\rho_{H2O}(\mu_s,\mu_v,\varphi)\,R_{865}(\mu_s,\mu_v,\varphi) + C_5 \quad (5)$$

where $C_3 = c_3 \cdot A$, $C_4 = c_3 \cdot B$ and C_5 is an adjustment constant. To be quite precise, we use a least squares method that minimizes the sum of squares of differences between the "true" and the estimated values of the shortwave reflectance. The NB-BB conversion is performed with respect to reflectance, that is thought to be preferable to a radiance regression [*Cess and Potter*, 1986].

3.2. Shortwave Albedos

[20] Let be $A_{443}(\mu_s, \mu_v, \varphi)$, $A_{670}(\mu_s, \mu_v, \varphi)$ and $A_{865}(\mu_s, \mu_v, \varphi)$ the "directional" values of albedo, that are the albedo values retrieved in a given viewing direction, at 443, 670, and 865 nm, respectively. They are derived from POLDER narrowband reflectance measurements by using radiative transfer modeling as explained in Part 1. These albedo values are free from gaseous absorption as the POLDER level 2 reflectance values. The SW "directional" albedo can be estimated as in equation (5) but by replacing the reflectance values by the albedo ones and the air mass factor m by an equivalent air mass factor M_i given by

$$M_i = 1/\mu_s + \eta_i \quad (6)$$

where η_i is the so-called diffusivity factor commonly used in the transmission modeling for taking into account the integration over viewing directions. Following *Lacis and Hansen* [1974], the best value is $\eta_1 = 1.9$ for ozone absorption and $\eta_2 = 1.66$ for water vapor absorption.

[21] The transmission function $T_{vis}(mU_{03})$ that appears in equation (5) is then simply replaced by $T_{vis}(M_1U_{03})$. For the water vapor absorption, the problem is a little more complicated. The reflectance ratio $\rho_{H2O}(\mu_s, \mu_v, \varphi)$ used in equation (4) can be considered as a water vapor transmission that is well approximated by

$$\rho_{H2O}(\mu_s,\mu_v,\varphi) = \exp\left[-\alpha(m\,U_{H2O})^{\beta}\right] \quad (7)$$

where α and β are constants and U_{H2O} represents the vertical column of water vapor. Replacing m by M_2 in the right-hand side of equation (7) involves replacing $\rho_{H2O}(\mu_s, \mu_v, \varphi)$ by

$$[\rho_{H2O}(\mu_s,\mu_v,\varphi)]^{\zeta(\mu_s,\mu_v,\varphi)} = \exp\left[-\alpha(M_2\,U_{H2O})^{\beta}\right] \quad (8)$$

with

$$\zeta(\mu_s,\mu_v,\varphi) = (M_2/m)^{\beta} \quad (9)$$

where the value of β (= 0.593) is fitted from line-by-line transmission calculations based on HITRAN database [*Rothman et al.*, 2003].

[22] Finally, the SW "directional" albedo is thus estimated from

$$A_{sw}(\mu_s,\mu_v,\varphi) = [C_1\,A_{443}(\mu_s,\mu_v,\varphi) + C_2\,A_{670}(\mu_s,\mu_v,\varphi)] \cdot T_{vis}(M_1U_{03}) + C_3\,A_{865}(\mu_s,\mu_v,\varphi) + C_4\,[\rho_{H2O}(\mu_s,\mu_v,\varphi)]^{\zeta(\mu_s,\mu_v,\varphi)}\,A_{865}(\mu_s,\mu_v,\varphi) + C_5 \quad (10)$$

where the coefficients C_1, C_2, ..., C_5 are the same as in equation (5). In this equation, the use of equivalent air mass factors is not rigorous but introduces a relative error estimated to no more than some tenths of a percent.

[23] The SW albedo $A_{sw}(\mu_s)$, that is the final result, is then deduced by weighted averaging of the different directional values of $A_{sw}(\mu_s, \mu_v, \varphi)$. The weights are functions of the viewing geometry and depend on the observed cloudiness, as explained in Part 1.

4. Determination of the Regression Coefficients

[24] The five coefficients C_i (i = 1, 5) used in equations (5) and (10) can be determined either theoretically or empirically. In the second approach the coefficients are determined from the comparison between the POLDER reflectances and the "true" SW reflectances measured by an ERB scanner. However, as there was no ERB scanner in flight during the ADEOS-1 period, the regression coefficients were previously determined from simulations.

4.1. Theoretical Approach

[25] The approach based on radiative transfer simulations was developed for ADEOS-1 POLDER [*Buriez et al.*, 1997]. To do that, we used the Global Atmospheric Model (GAME) developed by *Dubuisson et al.* [1996]. This radiative transfer code allows accurate treatment of scattering by aerosols, clouds and molecules in 4750 spectral intervals from 0.2 to 4 μm. Multiple scattering effects are treated using the Discrete Ordinates Method [*Stamnes et al.*, 1988]. Gaseous absorption is taken into account by using the exponential-sum fitting technique [*Wiscombe and Evans*, 1977].

[26] Narrowband and broadband albedo simulations were performed for five values of μ_s (from 0.2 to 1) and for two very different standard atmospheres: the tropical atmosphere and the subarctic winter atmosphere [*McClatchey et al.*, 1972]. Three surface models were considered: ocean, vegetation and sand. The calculations were performed for clear-sky situations with standard aerosol models [*World Meteorological Organization*, 1986] and for overcast situations corresponding to two cloud top pressures (200 and 900 hPa) and five cloud optical thicknesses (1.3, 3.6, 9.4, 23, and 125). Only liquid water cloud droplets with an effective radius of 10 μm were considered. This was consis-

Table 1. Coefficients Defined in Equations (5) and (10), Previously Derived From Radiative Transfer Simulations (Step 1) and Presently From Comparison to CERES Broadband Measurements (Step 2)

	C_1	C_2	C_3	C_4	C_5
Step 1	0.241	0.173	0.106	0.288	0.015
Step 2	0.193	0.260	0.129	0.244	0.020

tent with the cloud optical thickness retrieval method previously used for ADEOS-1 POLDER. From these simulations, the values of C_i (i = 1, 5) were derived by a least squares method. Although they were derived from albedo calculations, they can be applied also to reflectances by assuming the equivalence between equations (5) and (10).

[27] These values of C_i are reported in Table 1. The simple theoretical simulations used for their derivation do not pretend to reproduce the full radiative complexity of the atmosphere and surface. These coefficient values that are thus expected not to work well for real scenes were just temporary values by waiting the coincidence of an ERB scanner with the POLDER radiometer. Nevertheless, it will be interesting to compare some results obtained with them to those obtained from the following empirical approach.

4.2. Empirical Approach

[28] Now we take advantage of coincidences between ADEOS-2 POLDER and Terra CERES observations for deriving new regression coefficients. These coefficients are calculated by minimizing the sum of squares of the differences between the SW reflectances estimated from POLDER data by using equation (5) and the SW reflectances derived from CERES measurements.

[29] The values of C_i (i = 1, 5) were thus derived from all the 94,871 coincident data from April, July and October 2003, as described in section 2. These values are reported in Table 1 and can be compared to those obtained from the theoretical approach.

[30] About 99.4% of the variance of the SW reflectance is explained by the new regression based on equation (5). If only one channel was used, the explained variance would be 91.8%, 98.0%, 94.7% and 96.2%, for 443 nm, 670 nm, 865 nm and 910 nm, respectively. As already noted by several authors [e.g., *Lazlo et al.*, 1988; *Li and Leighton*, 1992; *Chakrapani et al.*, 2003], there is a high correlation between the SW and the visible channel but a multichannel combination significantly improves the broadband prediction, especially when no scene discrimination is prescribed as it is the case in our simple physically based regression with constant coefficients. Note also that our regression benefits from the presence of a water vapor channel on POLDER. The explained variance would be already 99.2% if only the two channels at 670 nm and 910 nm were used, while it would be 99.0% by using only the three channels at 443 nm, 670 nm and 865 nm.

5. Comparison Between POLDER and CERES SW Reflectances and Albedos From Codirectional Data

[31] In this section, we consider the 94,871 simultaneous collocated codirectional data used in the regression described in section 4.2. Main statistics of the comparisons between the POLDER SW reflectances (albedos) estimated by using the coefficients shown in Table 1 and the CERES SW reflectances (albedos) are reported in Table 2 (Table 3). Here, we do not take advantage of the multidirectional capacity of the POLDER instrument. The POLDER albedo values considered in this section are simply the "directional" albedo values, not yet the final albedo values. In Tables 2 and 3, "clear-sky" and "overcast" scenes correspond to 1° cells where all the POLDER pixels are declared clear and cloudy, respectively, by the cloud detection algorithm of the POLDER "ERB, Water Vapor, and Clouds" processing line [*Sèze et al.*, 1999]. Tables 2 and 3 present results for the complete data set corresponding to all the three months (April, July and October 2003). In order to assess the accuracy of the present regression fit, we also verified that very similar results are obtained by considering each month separately. On the other hand, an assessment of the quality of the regression model has been done by using data from an independent month (June 2003). In the two cases, monthly mean differences in reflectance and albedo remain always within ±0.5% (in relative value) away from the mean 3-month differences reported in Tables 2 and 3.

5.1. Shortwave Reflectances

[32] At first, consider quickly the results obtained with the previous coefficients based on a theoretical approach. The POLDER SW reflectance estimates present an overall relative bias of about −4%. This all-sky underestimation is slightly less important over ocean (−3.6%) than over

Table 2. Comparison Between the POLDER SW Reflectances Estimated by Using Coefficients Reported in Table 1 and the CERES SW Reflectances[a]

Scene	Number of Coincidences	Mean CERES Reflectance	Step 1		Step 2	
			Bias	RMS	Bias	RMS
All	94,871	0.270	−0.010 (−3.9%)	0.017 (6.2%)	0 (0.0%)	0.012 (4.3%)
Clear-sky over continent	4,962	0.178	−0.010 (−5.4%)	0.013 (7.5%)	−0.000 (−0.1%)	0.005 (3.0%)
Clear-sky over ocean	417	0.056	+0.004 (+6.4%)	0.004 (8.0%)	+0.005 (+9.0%)	0.006 (10.6%)
Partly cloudy over continent	7,033	0.211	−0.011 (−4.5%)	0.016 (6.7%)	−0.001 (−0.3%)	0.010 (4.2%)
Partly cloudy over ocean	18,546	0.199	−0.007 (−3.3%)	0.014 (7.1%)	+0.001 (+0.5%)	0.012 (5.9%)
Overcast over continent	21,445	0.459	−0.017 (−3.7%)	0.021 (4.6%)	+0.001 (+0.1%)	0.012 (2.7%)
Overcast over ocean	42,468	0.433	−0.017 (−4.0%)	0.022 (5.1%)	−0.002 (−0.4%)	0.014 (3.2%)

[a]BIAS corresponds to the mean POLDER minus CERES difference, and RMS to the root mean square difference. Observations correspond to April, July and October 2003.

Table 3. As in Table 2 but for the SW Albedos[a]

Scene	Number of Coincidences	Mean CERES Albedo	Step 1		Step 2	
			Bias	RMS	Bias	RMS
All	94,871	0.288	−0.005 (−1.7%)	0.016 (5.7%)	0.007 (+2.3%)	0.016 (5.6%)
Clear-sky over continent	4,962	0.186	−0.010 (−5.3%)	0.013 (7.1%)	−0.001 (−0.4%)	0.006 (3.0%)
Clear-sky over ocean	417	0.078	+0.004 (+5.2%)	0.005 (6.5%)	+0.006 (+8.3%)	0.007 (9.0%)
Partly cloudy over continent	7,033	0.226	−0.005 (−1.9%)	0.015 (6.4%)	+0.006 (+2.3%)	0.015 (6.2%)
Partly cloudy over ocean	18,546	0.224	−0.000 (−0.1%)	0.015 (6.6%)	+0.009 (+3.9%)	0.017 (7.6%)
Overcast over continent	21,445	0.468	−0.011 (−2.3%)	0.021 (4.5%)	+0.008 (+1.6%)	0.019 (4.1%)
Overcast over ocean	42,468	0.451	−0.012 (−2.7%)	0.020 (4.4%)	+0.005 (+1.0%)	0.016 (3.7%)

[a]Note that the POLDER albedo values considered here are simply the "directional" albedo values, not the final (weighted-averaged) albedo values.

continental surfaces (−4.3%) because of an overestimation over ocean under clear-sky conditions. As displayed on Figure 1, the slope of the scatterplot of POLDER SW reflectance estimates versus CERES measured reflectances is too small. Figure 2 shows that this default is highlighted when only the clear-sky cells are selected. It suggests that the bright surfaces such as deserts are particularly badly represented by the model used in the theoretical approach.

[33] Of course, better results are found when the present coefficients based on the empirical approach are used. The scatterplot of POLDER SW reflectances versus CERES ones presents a slope very close to unity not only for the whole data set (Figure 3) but also for the clear-sky situations (Figure 4 to be compared to Figure 2). The correlation appears to be satisfactory for all the situations except for the scarce oceanic areas that are fully cloud-free at the 1° regional scale (see Table 2). The root mean square (rms) difference between POLDER and CERES SW reflectances is in the range 0.005–0.014 depending on the scene type. Except for clear-sky ocean, this RMS difference is smaller than that obtained with the previous coefficients by 0.002–0.009 and the bias remains within ±0.002 (±0.5% in relative value), that is about ten times weaker than with the previous coefficients.

[34] Regressions (not shown) were also performed with coefficients that depend on geotype (ocean, continent) and cloudiness (clear sky, partly cloudy, overcast). Practically no additional improvement was found, except for the clear-sky oceanic scenes where the RMS difference became 0.002 instead of 0.006. Moreover, these scene-dependent regression coefficients present some negative values that are physically unclear. So, we prefer not to complicate the present regression and preserve the same coefficients whatever the scene type.

[35] Another point concerns the illumination and viewing conditions. The mean difference between POLDER and CERES SW reflectances tends to decrease with both solar and viewing zenith angle, as shown in Figures 5 and 6. However, these biases remain within ±0.005 (±1.6% in relative value), that is of the order of the state-of-the-art accuracy of ERB scanners [*Haeffelin et al.*, 2001; *Smith et al.*, 2006]. So, we prefer again to preserve the present regression as the introduction of angle-dependent coefficients improves only slightly the regression and would weaken the transfer from equation (5) to equation (10). Indeed, if the coefficients C_j were functions of the air mass factor, the role of the diffusivity factor introduced in

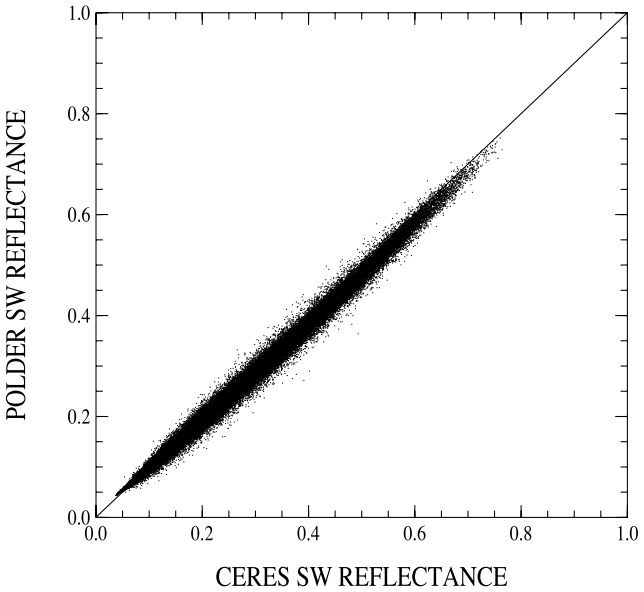

Figure 1. Scattergram of POLDER SW reflectances estimated by using previous coefficients (step 1) versus CERES SW reflectances. Observations correspond to April, July and October 2003.

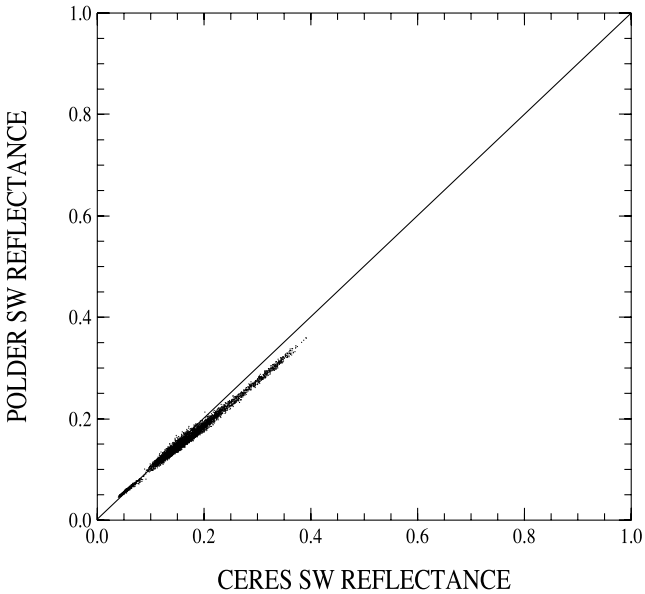

Figure 2. As in Figure 1 but only for clear-sky areas.

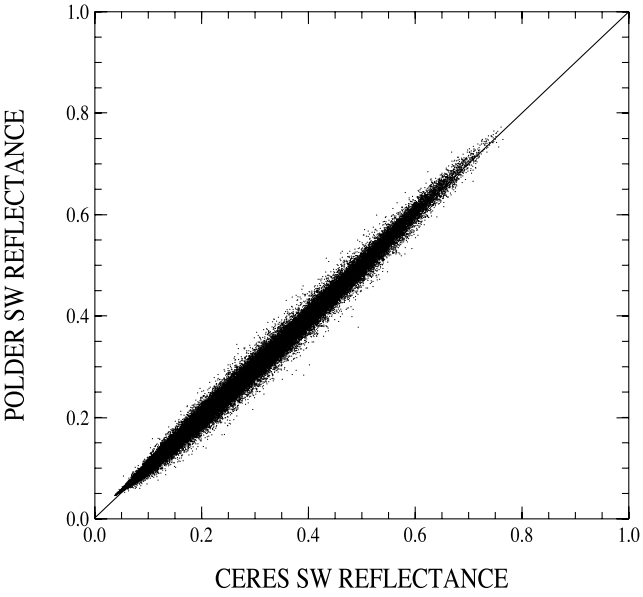

Figure 3. Scattergram of POLDER SW reflectances estimated by using present coefficients (step 2) versus CERES SW reflectances. Observations correspond to April, July and October 2003.

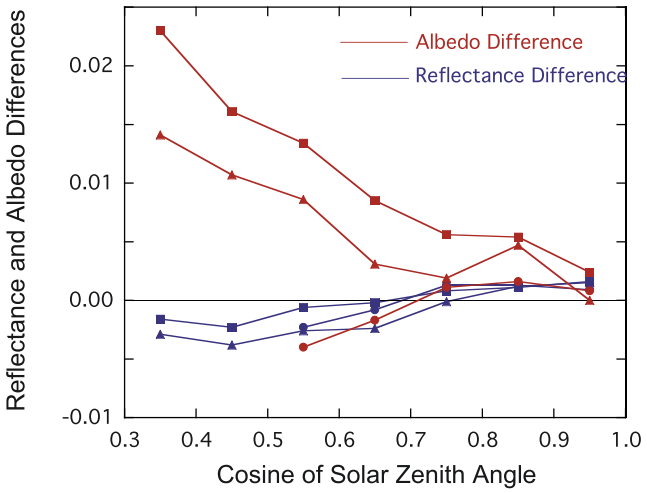

Figure 5. Mean differences between the POLDER SW reflectances ("directional" albedos) estimated by using present coefficients and CERES SW reflectances (albedos) as a function of the cosine of solar zenith angle, for clear-sky (circles), partly cloudy (squares) and overcast (triangles) conditions. Reflectance difference curves are blue while albedo differences curves are red. Each point corresponds to at least 200 coincidences.

equation (6) would be more important and could introduce more uncertainty than actually exists.

5.2. Shortwave Albedos

[36] When the POLDER and CERES albedo estimates are compared, the SW albedo scatterplots (not reported) are very similar to the SW reflectance scatterplots with a slightly larger dispersion. However, somewhat surprisingly, the RMS albedo difference between POLDER and CERES SW estimates is hardly weaker with the present approach than with the previous ones, while it is almost one and half times weaker in reflectance (see Tables 2 and 3). Moreover, the overall bias is weaker in albedo with the previous approach. Actually, the rather good performance of the previous regression is due to compensating effects: when there is no bias in reflectance, there is a relative bias of 2.3% in albedo; when there is a relative bias of −3.9% in reflectance, there is a relative bias of −1.7% in albedo, that is very close to (−3.9 + 2.3)%. This difference between the albedo and the reflectance bias is practically inevitable whatever the values of the coefficients C_j, which have to be physically the same in equations (5) and (10). Indeed, the ratio between the POLDER narrowband albedos and reflectances, both free from gaseous absorption, is around 1.10 for the three POLDER channels, while the CERES broadband albedo/reflectance ratio is only 1.065. Thus, when the

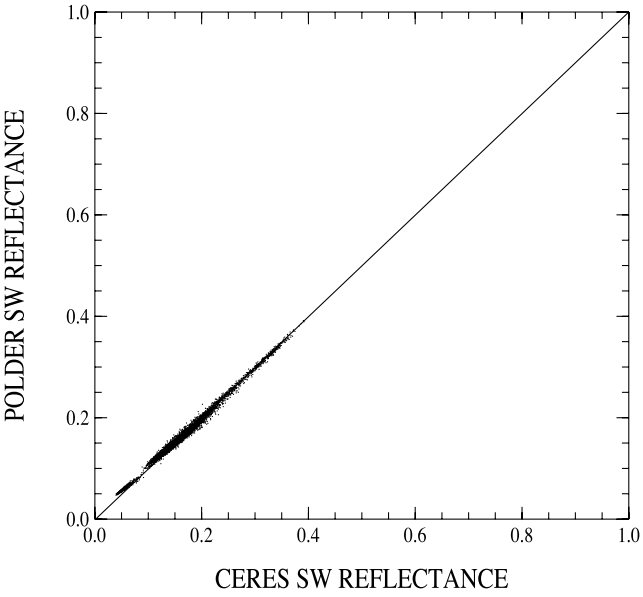

Figure 4. As for Figure 3 but only for clear-sky areas.

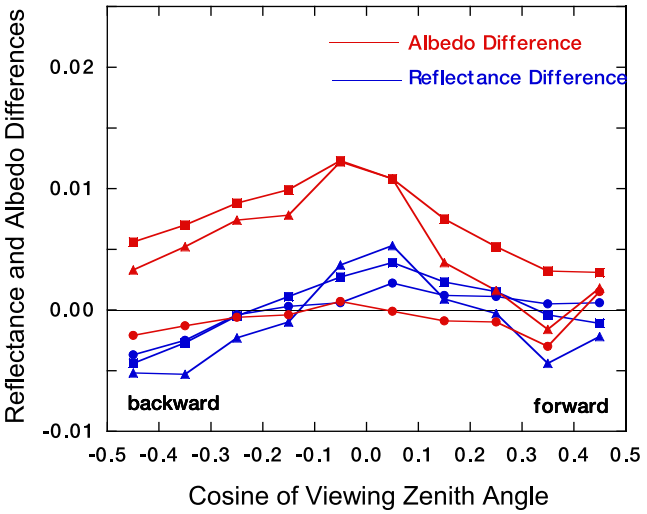

Figure 6. As in Figure 5 but as a function of the cosine of viewing zenith angle.

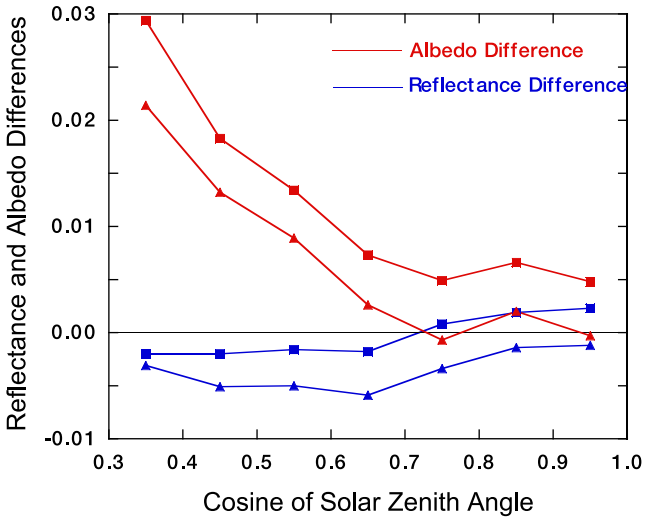

Figure 7. As in Figure 5 but by considering only the liquid water cloud scenes.

regression is transposed from reflectance to albedo, the POLDER/CERES ratio would increase by almost 4% if there was no gaseous absorption. Practically, it increases by around 2–3% whatever the regression coefficient values. In all the following, we focus on the present regression derived from the comparison between POLDER and CERES reflectances.

[37] Unlike the measured SW reflectance, the CERES SW albedo is only an estimate, which is based on ADM models. The overall relative RMS difference between POLDER and CERES SW albedo estimates is 5.6%. By treating the errors as random and considering a 4.3% uncertainty due to the POLDER NB-BB conversion, the RMS difference due to the POLDER and CERES reflectance-to-albedo conversions is 3.6%. These values have to be compared to the CERES SW albedo consistency of 5.3% between nadir and oblique viewing zenith angles estimated from a combination of CERES, Multiangle Imaging Spectroradiometer (MISR) [*Diner et al.*, 1998] and MODIS measurements [*Loeb et al.*, 2006, 2007]. This suggests that, for given 1°-regional instantaneous data, there is no evidence whether the CERES or the POLDER SW albedo estimate is better. However, when largely averaging over space and time, the uncertainty due to the CERES SSF ADMs is expected to be only some tenths of a percent [*Loeb et al.*, 2007]. Thus, if the CERES calibration is assumed to be "perfect," the mean POLDER all-sky albedo estimated with the present regression coefficients is expected to be overestimated by about 2% compared to reality.

[38] Now consider the clear-sky situations. Except in the hot spot area, the angular reflectance distributions of continental surfaces are generally nearly flat. Thus the reflectance-to-albedo conversion is expected to be accurate under clear-sky conditions over continents as well by the ADM method as by our modeling approach described in Part 1. In fact, the CERES and the POLDER albedo estimates are in very good agreement with no significant mean difference and a RMS difference of only 0.006 (3%). Concerning the clear-sky oceanic situations, the disagreement between the CERES and the POLDER SW albedo estimates is almost only related to the one observed for the reflectances: the relative POLDER-CERES bias is close to 9% both in reflectance and in albedo. Then, the CERES and the POLDER reflectance-to-albedo conversion can be considered as very consistent for all the clear-sky situations.

[39] For the overcast and partly cloudy scenes, the mean POLDER-CERES albedo difference is around 0.005–0.009. The behavior of the POLDER-CERES albedo differences as a function of the viewing direction is very close to that of the reflectance differences, with a very slight difference between the forward and the backward direction (see Figure 6). On the other hand, unlike the cloudy-sky reflectance difference, the mean cloudy-sky albedo difference increases notably with the solar zenith angle: from nearly zero at zenith up to ~0.02 at low solar elevations (see Figure 5).

[40] As the expected reason of the disagreement between POLDER and CERES is the weakness of the plane-parallel assumption for heterogeneous cloudy scenes, we select the cloudy cells over which the relative standard deviation of the CERES reflectance measurements is weaker than 10%. By doing so, we retain 42% of the overcast scenes and 17% of the partly cloudy scenes. The albedo RMS difference is 0.013 (3.7%) for these 21655 "homogeneous" scenes, to be compared to 0.017 (5.6%) for the whole of the cloudy scenes. In the same way, the mean albedo difference is reduced to 0.0036 (1.0%) that is twice weaker than for the whole of the cloudy scenes and its variation as a function of the solar zenith angle is also twice reduced. Thus we can consider that the CERES and the POLDER albedo estimates tend to the same value as the scene tends to be fully homogeneous. Note that this conclusion cannot be drawn when the old regression coefficients are used. Indeed, the error compensation, which explains the relatively good performance of the old regression, works less well for the homogeneous scenes than for the whole of the cloudy scenes.

[41] To examine the influence of the cloud thermodynamic phase, we select the 1° cells corresponding to liquid water cloud scenes by using the cloud phase retrieved from POLDER polarization measurements [*Goloub et al.*, 2000]. Figure 7 confirms the solar zenith angle dependence of the POLDER-CERES albedo difference for the 20,522 cloudy cells composed of pixels for which the cloud phase, when determined, is liquid. In a similar manner, we select 10,896 cells corresponding to ice cloud scenes. The solar zenith angle dependence of the POLDER-CERES albedo difference is reported in Figure 8. This dependence appears weak and it is not sure that the small peak observed for the overcast ice clouds at $\mu_s \sim 0.85$ is significant. For the ice cloud situations, the POLDER-CERES albedo difference remains around only 0.002 (0.8%). With regard to the reflectance-to-albedo conversion, the plane-parallel model thus appears to be more adequate for ice clouds than for liquid water clouds. This does not prevent the well-known "plane-parallel bias" [*Cahalan et al.*, 1994] due to the relation between cloud optical thickness and albedo from being quite important for ice clouds [*Carlin et al.*, 2002; *Oreopoulos and Cahalan*, 2005]. Nevertheless, this tends to confirm the good performance of the Inhomogeneous Hexagonal Monocrystal model [*C.-Labonnote et al.*, 2001;

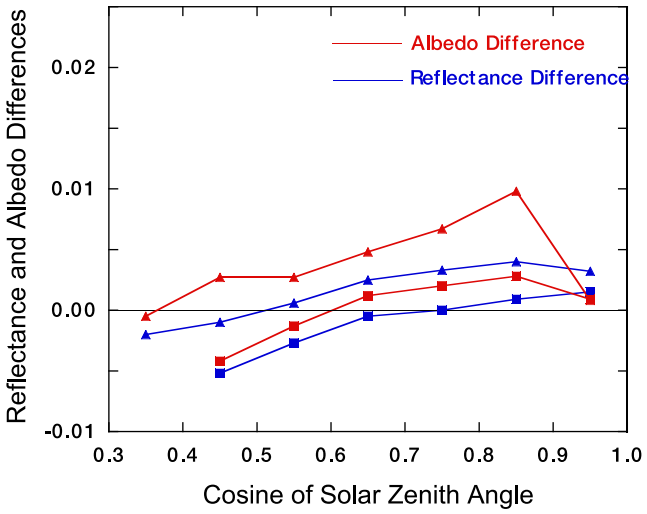

Figure 8. As in Figure 5 but by considering only the ice cloud scenes.

Baran and C.-Labonnote, 2005], which is used for deriving the narrowband albedos in Part 1.

6. Comparison Between POLDER and CERES SW Albedos at the Global Scale

[42] So far, we consider only codirectional POLDER and CERES data. It is needed for reflectance comparisons but not for albedo comparisons. Now, we compare POLDER and CERES SW albedo estimates whatever the viewing directions. Thus we shall no longer use the POLDER SW "directional" albedo $A_{sw}(\mu_s, \mu_v, \varphi)$ as in the preceding section, but the POLDER SW albedo $A_{sw}(\mu_s)$, which results from a weighted averaging of the different values of $A_{sw}(\mu_s, \mu_v, \varphi)$. Note that, concerning CERES, the albedo and the "directional" albedo are undistinguishable since, during a satellite pass, a given area is viewed under only one direction.

[43] Preliminarily, consider again the only 94,871 data used in section 5. As expected, when the POLDER "directional" albedos are replaced by the POLDER weighted-averaged albedos, the slope of the POLDER-CERES SW albedo difference as a function of the viewing zenith angle significantly decreases: roughly by a factor of two. Indirectly, the slope of the albedo difference as a function of the solar zenith angle also decreases but only by one third. Finally the mean and RMS albedo differences decrease overall by only one tenth.

[44] When all the coincident data, not necessarily codirectional, are retained, there is about three times more data. For these 266,044 coincidences, the POLDER-CERES SW albedo differences remain of the same order as above. The mean difference is 0.006 (2.2%) and the RMS difference is 0.015 (5.5%). It is also the case for the independent month (June 2003) with mean and RMS differences of 0.005 (1.9%) and 0.014 (5.4%), respectively.

[45] In a recent paper, *Sun et al.* [2006] estimate the MISR SW albedo from a combination of the MISR multi-angle measurements and the plane-parallel theory. Their approach is different from ours but clearly presents similarities. For the overcast oceanic 1° regions they consider, they found a mean MISR-CERES albedo difference of 0.8% and a RMS difference of 4.3%. When we select the 46,406 overcast oceanic scenes among the 266,044 POLDER-CERES coincidences, the mean POLDER-CERES albedo difference is 0.8% and the RMS difference is 3.7%. Despite the differences in data and methods and the errors due to the NB-BB conversion, the remarkable consistency between the MISR-CERES and the POLDER-CERES albedo differences gives us some confidence in our results.

[46] Because of the solar zenith angle dependence discussed in section 5, the POLDER-CERES SW albedo difference presents a latitudinal dependence. Figure 9 shows this mean albedo difference as a function of latitude for April, July and October 2003. For June 2003, the mean albedo difference (not reported) is very similar to that of July 2003 with values slightly weaker.

[47] In order to compare the POLDER and CERES estimates in terms of fluxes, the instantaneous SW albedo differences are converted into instantaneous SW flux differences by means of equation (2) and then into equivalent 24-hour SW flux differences by applying a scaling factor. This scaling factor is calculated for each 1° cell and for each month. It is approximated by the ratio between the monthly mean daily SW flux issued from the POLDER level 3 product [*Viollier et al.*, 2002] and the monthly mean instantaneous SW flux. Figure 10 presents the latitudinal variations of the resulting monthly SW flux difference between CERES and POLDER. On Figure 10 are reported the mean and the RMS difference resulting from an average of the 1° cell monthly mean flux over 1° zonal belts. The monthly mean SW flux difference varies little according to the month: on a global average, the monthly mean difference is around 2.0–2.2 W m^{-2} for each month considered. Moreover, it varies relatively little according to the latitude. This is consistent with the solar zenith angle

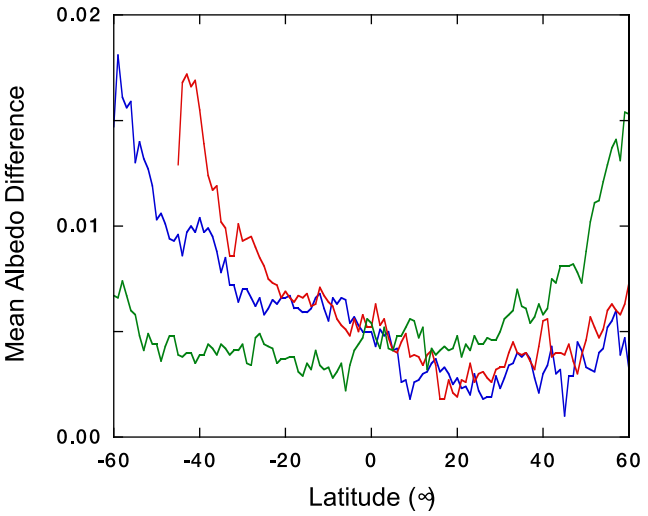

Figure 9. Mean difference between the POLDER SW (weighted averaged) albedos estimated by using present coefficients and CERES SW albedos as a function of latitude. Observations correspond to April 2003 (blue curve), July 2003 (red curve) and October 2003 (green curve).

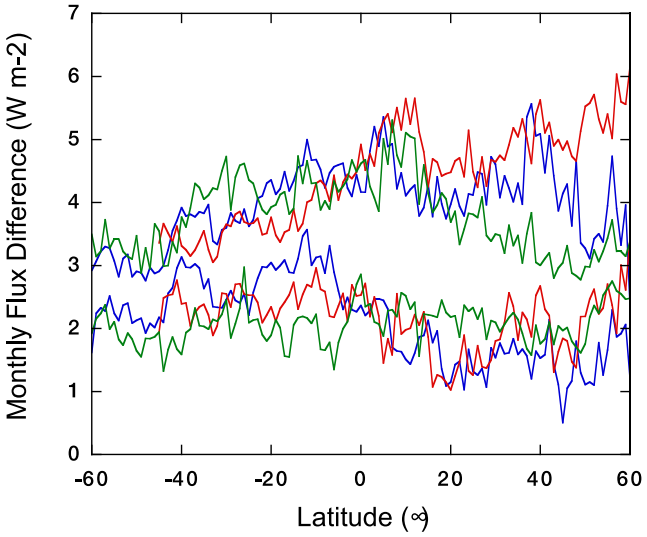

Figure 10. Monthly SW flux difference between POLDER and CERES as a function of latitude. Observations correspond to April 2003 (blue curves), July 2003 (red curves) and October 2003 (green curves). Top and bottom curves represent mean and RMS differences, respectively.

dependence of the albedo difference reported in section 5, which is largely reduced when the albedo difference is multiplied by the cosine of the solar zenith angle. This SW flux bias that is expected to be due to the plane-parallel hypothesis, is to be related to the recent work of *Loeb et al.* [2007] who estimated mean TOA flux errors made by using plane-parallel model SW ADMs. We found a mean SW flux bias roughly comparable on a global average, but with zonal variations noticeably less marked. In particular, *Loeb et al.* [2007] report negative differences in the subtropical regions where the Sun is able to reach high solar elevations, whereas Figure 10 shows no negative bias between POLDER and CERES SW fluxes. We do not find such a negative bias either when considering only liquid water cloud scenes as *Loeb et al.* [2007] do. We find no evidence to explain the difference of sign in the flux bias obtained in subtropical regions. Note that the relative differences between the MISR and CERES SW albedos show no systematic dependence upon latitude [*Sun et al.*, 2006].

7. Summary and Conclusions

[48] In Part 1 of this series, spectral albedos at 443 nm, 670 nm and 865 nm were derived from POLDER reflectance measurements by using a plane-parallel model. In this study, these spectral albedos are converted to SW albedos by using a NB-BB conversion analysis based on simultaneous collocated codirectional CERES and POLDER data acquired during April, July and October 2003. As the regression equation coefficients are determined, not from albedo estimates, but from reflectance measurements, the POLDER SW albedo estimates are independent from CERES except for calibration. In particular they are totally independent of the CERES ADM models.

[49] In our simple and physically based regression equation, the values at 443 and 670 nm are considered as representative of the UV-visible spectral range, and the value at 865 nm representative of the near infrared, except for the gaseous absorption. The solar ozone absorption is estimated from TOMS ozone data while the solar water vapor absorption is estimated from the POLDER 910-to-865 nm reflectance ratio. The regression equation coefficients that are the same for the reflectances and the albedos are fixed to be independent of scene type and illumination and viewing directions.

[50] In order to reduce uncertainties associated to footprint differences between CERES and POLDER, data are averaged over equal-area regions which have a size of 1° latitude by 1° longitude at the equator. By assuming the CERES reflectance measurements are not affected by measurement errors, the relative accuracy in 1° regional instantaneous SW reflectance from the present regression is 4.3%. That is about one and a half times better than with the same regression equation but previous theoretically based coefficients. Practically, except for some clear-sky oceanic areas, the present regression appears accurate enough, given the state-of-the-art accuracy of ERB scanners. For example, *Haeffelin et al.* [2001] compared ScaRaB and CERES SW radiances at 1° regional scale and found a relative RMS difference of 10%.

[51] When transposed from codirectional reflectance measurements to codirectional albedo estimates, the present regression gives a POLDER-CERES RMS difference of 5.6% in relative value. Note that the previous theoretically based regression coefficients used in particular by *Viollier et al.* [2002] for deriving the SW albedo at the global scale gives overall practically the same POLDER-CERES RMS difference than the present regression, but in fact because of compensating errors. The POLDER-CERES SW albedo difference is slightly reduced (by one tenth) when the POLDER SW albedo is derived from all the available viewing directions (up to 14 directions), rather than only from the cross-track direction. This POLDER-CERES difference in instantaneous SW albedo appears quite acceptable, given the SW albedo RMS difference of 5–6% observed between CERES observations at nadir and at oblique viewing zenith angles [*Loeb et al.*, 2006, 2007]. Moreover, the remarkable consistency between the POLDER-CERES albedo comparison and the MISR-CERES albedo comparison performed for overcast oceanic situations [*Sun et al.*, 2006] gives us some confidence in our results.

[52] For clear-sky situations, the CERES and the POLDER reflectance-to-albedo conversion are very consistent. On the contrary, for cloudy situations, the POLDER SW albedo estimates are biased compared to the CERES ones. This albedo bias increases notably with the solar zenith angle, from nearly zero at zenith up to about 0.02 (5% in relative value) at solar zenith angles around 70°. This albedo bias is thought to be due, for a large part, to our plane-parallel assumption (see Part 1) that can be crucial for the heterogeneous cloud scenes. Indeed, the albedo bias is significantly reduced (by a factor of two) when only the most homogeneous cloudy scenes (about a quarter of the whole cloudy scenes) are retained. It is also relatively weak (about 0.002, less than 0.8% in relative value) when only ice clouds are considered.

[53] The resulting monthly mean SW flux difference between POLDER and CERES is about 2 W m^{-2}, that is of the same order as the difference between CERES ERB-like and SSF fluxes [*Loeb et al.*, 2007]. The observed SW flux bias is to be related to the recent work of *Loeb et al.* [2007] who estimated mean TOA flux errors made by using plane-parallel model SW ADMs. We found a mean SW flux bias roughly comparable on a global average, but with zonal variations noticeably less marked.

[54] Further analyses are required to explain such a discrepancy. In the near future, further comparisons will be carried out from POLDER on Polarization and Anisotropy of Reflectances for Atmospheric Sciences coupled with Observations from a Lidar (PARASOL) and CERES on Aqua, both parts of the afternoon satellite constellation known as the A-train. Yet, this study demonstrates the overall consistency between both experiments. In any case, this conclusion would not reduce the need of onboard calibration systems like those used by CERES and other radiation budget experiments. They are necessary for long-term Earth observation and climate studies.

[55] **Acknowledgments.** This work was supported by CNES and the Région Nord-Pas de Calais. The POLDER level 2 data were obtained from the French Interactions Clouds Aerosols Radiations Etc (ICARE) Data Management and Processing Center. The CERES SSF data were obtained from the NASA Langley Research Center Atmospheric Sciences Data Center. The authors would like to thank N. G. Loeb for critically reading the original manuscript and for helpful information about CERES. They also gratefully acknowledge the three anonymous referees for their helpful comments and suggestions.

References

Anderson, G. P., F. X. Kneizys, E. P. Shettle, L. W. Abreu, J. H. Chetwynd, R. E. Huffman, and L. A. Hall (1990), UV spectral simulations using LOWTRAN 7, in *Atmospheric Propagation in the UV, Visible, IR and MM-Wave Region and Related Systems Aspects*, *AGARD Conf. Proc. 454*, 9 pp., Proceedings of the AGARD Electromagnetic Wave Propagation Panel Symposium, Copenhagen, 9–13 Oct. 1989.

Baker, G. A. (1965), The theory and application of the Padé approximant method, *Adv. Theor. Phys.*, vol. 1, edited by K. A. Brueckner, pp. 1–58, Elsevier, New York.

Baran, A. J., and L. C.-Labonnote (2005), On the reflection and polarisation properties of ice cloud, *J. Quant. Spectrosc. Radiat. Transfer*, *100*, 41–45, doi:10.1016/j.jqsrt.2005.11.062.

Barnes, W. L., T. S. Pagano, and V. V. Salomonson (1998), Prelaunch characteristics of the Moderate Resolution Imaging Spectroradiometer (MODIS) on EOS-AM1, *IEEE Trans. Geosci. Remote Sens.*, *36*, 1088–1100.

Buriez, J. C., C. Vanbauce, F. Parol, P. Goloub, M. Herman, B. Bonnel, Y. Fouquart, P. Couvert, and G. Seze (1997), Cloud detection and derivation of cloud properties from POLDER, *Int. J. Remote Sens.*, *18*, 2785–2813.

Buriez, J. C., F. Parol, C. Cornet, and M. Doutriaux-Boucher (2005), An improved derivation of the top-of-atmosphere albedo from POLDER/ADEOS-2: Narrowband albedos, *J. Geophys. Res.*, *110*, D05202, doi:10.1029/2004JD005243.

Cahalan, R. F., W. Ridgway, W. J. Wiscombe, T. L. Bell, and J. B. Snider (1994), The albedo of fractal stratocumulus clouds, *J. Atmos. Sci.*, *51*, 2434–2455.

Carlin, B., Q. Fu, U. Lohmann, J. M. Comstock, G. G. Mace, and K. Sassen (2002), High cloud horizontal inhomogeneity and solar albedo bias, *J. Clim.*, *15*, 2321–2339.

Cess, R. D., and G. L. Potter (1986), Narrow- and broad-band satellite measurements of shortwave radiation: Conversion simulations with a general circulation model, *J. Clim. Appl. Meteorol.*, *25*, 1977–1984.

Chakrapani, V., P. Minnis, D. R. Doelling, and M. M. Khaiyer (2003), New visible to broadband shortwave conversions for deriving albedos from GOES-8 over the ARM-SGP, in *Thirteenth ARM Science Team Meeting Proceedings*, Atmos. Radiat. Measuring Program, Dep. Of Energy, Broomfield, Colo., March 31–April 4. [Available on-line from http://www.arm.gov/publications/]

C.-Labonnote, L., G. Brogniez, J. C. Buriez, M. Doutriaux-Boucher, J. F. Gayet, and A. Macke (2001), Polarized light scattering by inhomogeneous hexagonal monocrystals. Validation with ADEOS-POLDER measurements, *J. Geophys. Res.*, *106*, 12,139–12,153.

Cox, C., and W. Munk (1956), Slopes of the sea surface deduced from photographs of the sun glitter, *Bull. Scripps Inst. Oceanogr.*, *6*, 401–488.

Deschamps, P. Y., F. M. Breon, M. Leroy, A. Podaire, A. Bricaud, J. C. Buriez, and G. Seze (1994), The POLDER mission: Instrument characteristics and scientific objectives, *IEEE Trans. Geosci. Remote Sens.*, *32*, 598–615.

Diner, D. J., et al. (1998), Multiangle Imaging Spectroradiometer (MISR) instrument description and experiment overview, *IEEE Trans. Geosci. Remote Sens.*, *36*, 1072–1087.

Dubovik, O., B. Holben, T. F. Eck, A. Smirnov, Y. J. Kaufman, M. D. King, D. Tanré, and I. Slutsker (2002), Variability of absorption and optical properties of key aerosol types observed in worldwide locations, *J. Atmos. Sci.*, *59*, 590–608.

Dubuisson, P., J. C. Buriez, and Y. Fouquart (1996), High spectral resolution solar radiative transfer in absorbing and scattering media: Application to the satellite simulation, *J. Quant. Spectrosc. Radiat. Transfer*, *55*, 103–126.

Duvel, J. P., S. Bouffiès-Cloché, and M. Viollier (2000), Determination of shortwave Earth reflectances from visible radiance measurements: Error estimate using ScaRaB data, *J. Appl. Meteorol.*, *39*, 957–970.

Geier, E. B., R. N. Green, D. P. Kratz, P. Minnis, W. F. Miller, S. K. Nolan, and C. B. Franklin (2003), Single satellite footprint TOA/surface fluxes and clouds (SSF) collection document, Release 2, version 1, Natl. Aeronaut. and Space Admin, Langley Res. Cent., Hampton, Va. [Available on-line at http://asd-www.larc.nasa.gov/ceres/collect_guide/SSF_CG.pdf]

Goloub, P., M. Herman, H. Chepfer, J. Riedi, G. Brogniez, P. Couvert, and G. Sèze (2000), Cloud thermodynamical phase determination from the POLDER spaceborne instrument, *J. Geophys. Res.*, *105*, 14,747–14,759.

Haeffelin, M., B. A. Wielicki, J. P. Duvel, K. Priestley, and M. Viollier (2001), Intercalibration of CERES and ScaRaB Earth radiation budget datasets using temporally and spatially collocated radiance measurements, *Geophys. Res. Lett.*, *28*, 167–170.

Hagolle, O., P. Goloub, P. Y. Deschamps, H. Cosnefroy, X. Briottet, T. Bailleul, J. M. Nicolas, F. Parol, B. Lafrance, and M. Herman (1999), Results of POLDER in-flight calibration, *IEEE Trans. Geosci. Remote. Sens.*, *37*, 1550–1566.

Hautecoeur, O., and M. Leroy (1998), Surface bidirectional reflectance distribution function observed at global scale by POLDER/ADEOS, *Geophys. Res. Lett.*, *25*, 4197–4200.

Hucek, R., and H. Jacobowitz (1995), Impact of scene dependence on AVHRR albedo models, *J. Atmos. Oceanic Technol.*, *12*, 697–711.

Kandel, R., et al. (1998), The ScaRaB earth radiation budget dataset, *Bull. Am. Meteorol. Soc.*, *79*, 765–783.

Lacis, A. A., and J. E. Hansen (1974), A parameterization for the absorption of solar radiation in the Earth's atmosphere, *J. Atmos. Sci.*, *31*, 118–133.

Lazlo, I., H. Jacobowitz, and A. Gruber (1988), The relative merits of narrowband channels for estimating broadband albedos, *J. Atmos. Oceanic Technol.*, *5*, 757–773.

Li, Z., and H. G. Leighton (1992), Narrowband to broadband conversion with spatially autocorrelated reflectance measurements, *J. Appl., Meteorol.*, *31*, 653–670.

Li, Z., and A. Trishchenko (1999), A study towards an improved understanding of the relation between visible and SW albedo measurements, *J. Atmos. Oceanic Technol.*, *17*, 347–360.

Loeb, N. G., K. J. Priestley, D. P. Kratz, E. B. Geier, R. N. Green, B. A. Wielicki, P. O'R. Hinton, and S. K. Nolan (2001), Determination of unfiltered radiances from the Clouds and the Earth's Radiant Energy System (CERES) instrument, *J. Appl. Meteorol.*, *40*, 822–835.

Loeb, N. G., S. Kato, and B. A. Wielicki (2002), Defining top-of-atmosphere flux reference level for Earth radiation budget studies, *J. Clim.*, *15*, 3301–3309.

Loeb, N. G., S. Kato, K. Loukachine, and N. Manalo-Smith (2005), Angular distribution models for top-of-atmosphere radiative flux estimation from the Clouds and the Earth's Radiant Energy System instrument on the Terra satellite. Part I: Methodology, *J. Atmos. Oceanic Technol.*, *22*, 338–351, doi:10.1175/JTECH1712.1.

Loeb, N. G., W. Sun, W. F. Miller, K. Loukachine, and R. Davies (2006), Fusion of CERES, MISR, and MODIS measurements for top-of-atmosphere radiative flux validation, *J. Geophys. Res.*, *111*, D18209, doi:10.1029/2006JD007146.

Loeb, N. G., S. Kato, K. Loukachine, N. Manalo-Smith, and D. R. Doelling (2007), Angular distribution models for top-of-atmosphere radiative flux estimation from the Clouds and the Earth's Radiant Energy System instrument on the Terra satellite. Part II: Validation, *J. Atmos. Oceanic Technol.*, *24*, 564–584.

McClatchey, R. A., R. W. Fenn, J. E. A. Selby, F. E. Voltz, and J. S. Garing (1972), Optical properties of the atmosphere, *AFCRL-72-0497*, 108 pp., Air Force Geophys. Lab., Hanscom Air Force Base, Mass.

Minnis, P., and E. F. Harrison (1984), Diurnal variability of regional cloud and clear-sky radiative parameters derived from GOES data. Part III: November 1978 radiative prameters, *J. Clim. Appl. Meteorol.*, *23*, 1032–1051.

Minnis, P., W. L. Smith Jr., D. P. Garber, J. K. Ayers, and D. R. Doelling (1995), Cloud properties derived from GOES-7 for spring 1994 ARM intensive observing period using version 1.0.0 of ARM satellite data analysis program, *NASA RP-1366*, 58 pp., Natl. Aeronaut. and Space Admin, Langley Res. Cent., Hampton, Va.

Oreopoulos, L., and R. F. Cahalan (2005), Cloud inhomogeneity from MODIS, *J. Clim.*, *18*, 5110–5124, doi:10.1175/JCLI3591.1.

Rothman, L. S., et al. (2003), The HITRAN molecular spectroscopic database: Edition of 2000 including updates through 2001, *J. Quant. Spectrosc. Radiat. Transf.*, *82*, 5–44.

Salomonson, V. V., W. L. Barnes, P. W. Maymon, H. E. Montgomery, and H. Ostrow (1989), MODIS: Advanced facility instrument for studies of the earth as a system, *IEEE Trans. Geosci. Remote Sens.*, *27*, 145–153.

Sèze, G., C. Vanbauce, J. C. Buriez, F. Parol, and P. Couvert (1999), Cloud cover observed simultaneously from POLDER and METEOSAT, *Phys. Chem. Earth*, *24*, 921–926.

Smith, G. L., Z. P. Szewczyk, D. A. Rutan, and R. B. Lee III (2006), Comparison of measurements from satellite radiation budget instruments, *J. Geophys. Res.*, *111*, D04101, doi:10.1029/2005JD006307.

Stamnes, K., S.-C. Tsay, W. Wiscombe, and K. Jayaweera (1988), Numerically stable algorithm for discrete-ordinate-method radiative transfer in multiple scattering and emitting layered media, *Appl. Opt.*, *27*, 2502–2509.

Sun, W., N. G. Loeb, R. Davies, K. Loukachine, and W. F. Miller (2006), Comparison of MISR and CERES top-of-atmosphere albedo, *Geophys. Res. Lett.*, *33*, L23810, doi:10.1029/2006GL027958.

Trishchenko, A., and Z. Li (1998), Use of ScaRaB measurements for validating a GOES-based TOA radiation product, *J. Appl. Meteorol.*, *35*, 591–605.

Vesperini, M., and Y. Fouquart (1994), Determination of broad-band shortwave fluxes from the Meteosat visible channel by comparison to ERBE, *Beitr. Phys. Atmos.*, *67*, 121–131.

Viollier, M., C. Standfuss, and F. Parol (2002), Monthly means of reflected solar flux from POLDER (ADEOS-1) and comparison with ERBE, ScaRaB and CERES, *Geophys. Res. Lett.*, *29*(10), 1503, doi:10.1029/2001GL014255.

Viollier, M., R. Kandel, and P. Raberanto (2004), Combination of ScaRaB-2 and CERES with Meteosat-5 to remove time sampling bias and improve radiation budget estimations in the INDOEX region, *J. Geophys. Res.*, *109*, D05105, doi:10.1029/2003JD003947.

Wielicki, B. A., B. R. Barkstrom, E. F. Harrison, R. B. Lee III, G. L. Smith, and J. E. Cooper (1996), Clouds and the Earth's Radiant Energy System (CERES): An earth observing system experiment, *Bull. Am. Meteorol. Soc.*, *77*, 853–868.

Wielicki, B. A., et al. (2002), Evidence for large decadal variability in the Tropical mean radiative energy budget, *Science*, *295*, 841–844, doi:10.1126/science.1065837.

Wiscombe, W., and J. Evans (1977), Exponential-sum fitting of radiative transmission functions, *J. Comput. Phys.*, *24*, 416–444.

World Meteorological Organization (1986), A preliminary cloudness standard atmosphere for radiation computation, *Rep. no 24, WCP-112*, 53 pp., World Meteorol. Org., Geneva.

J.-C. Buriez and F. Parol, Laboratoire d'Optique Atmosphérique, UMR CNRS 8518, Université des Sciences et Technologies de Lille, F-59655 Villeneuve d'Ascq, France.

Z. Poussi, CGTD, Interactions Clouds Aerosols Radiations Etc., Université des Sciences et Technologies de Lille, F-59655 Villeneuve d'Ascq, France.

M. Viollier, Laboratoire de Météorologie Dynamique, CNRS, Ecole Polytechnique, F-91128 Palaiseau, France.